Langmuir

Article

pubs.acs.org/Langmuir

Electrostatic Polyion Micelles with Fluorescence and MRI Dual Functions

Zheng Wu, Jianbin Huang,* and Yun Yan*

Beijing National Laboratory for Molecular Sciences (BNLMS), State Key Laboratory for Structural Chemistry of Unstable and Stable Species, College of Chemistry and Molecular Engineering, Peking University, Beijing 100871, China

ABSTRACT: We report in this work the formation of fluorescence and MRI bimodal imaging nanoparticles achieved by electrostatic self-assembly. The nanoparticles are micelles formed with Gd^{3+} ion, a bisligand that contains aggregation induced emission (AIE) group, and a block copolymer. The coordination between the Gd^{3+} ion and the bisligand produces a negatively charged coordination complex, which interacted with the positive-neutral block copolymer to form polyion micelles. The micelles exhibit considerable fluorescence owing to the rotation restriction of the AIE group; meanwhile, the longitudinal relaxation of water was significantly slowed down which provide T_1 contrast for magnetic resonance imaging. *In vitro* fluorescence imaging and *in vivo* MRI measurements verified this micelle indeed exhibit dual imaging ability. We expect that this orthogonal imaging may provide more accurate diagnosis in practical applications and will pave the way for the development of an advanced technique for diagnosis.

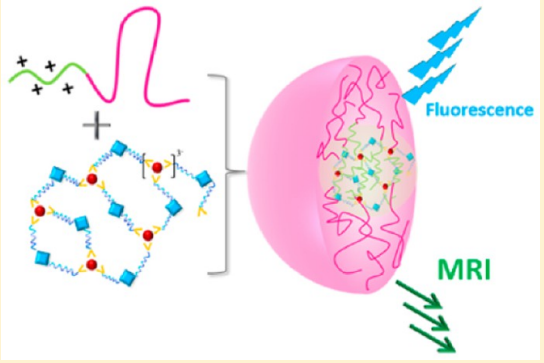

INTRODUCTION

The past decades have witnessed the thriving of molecular imaging for disease detection because of its noninvasive, real time, and three-dimensional imaging of physiological conditions.[1,2] Up to date, there are already various kinds of imaging methods, such as magnetic resonance imaging (MRI),[3,4] fluorescence imaging (FI),[5] computed tomography (CT),[6] ultrasound,[7] nuclear imaging,[8] and so on. However, one should be careful with diagnosis based on one imaging method since each imaging modality has its specific advantages and drawbacks. For instance, the method of MRI is characterized by high resolution but low sensitivity, whereas FI has high sensitivity but low resolution.[9,10] A recent trend is therefore to develop bi- or multimodal imaging systems, which fuse the advantages of different molecular imaging methods into one probe.[11,12] This concept is essentially important for more accurate diagnosis since no single modality is perfect and sufficient for both high resolution and sensitivity.

Herein we report an advanced micellar system which exhibits MRI/FI dual ability. The micelles were electrostatic assemblies between a negatively charged coordination complex and a positively charged block copolymer. The coordination complex was built with Gd^{3+} and a bisligand which contains an aggregation induced emission (AIE) group in water.[13−15] Since Gd^{3+} significantly shortens the T_1 mode relaxation of nearby water molecules,[16] the contrast between areas with and without Gd^{3+} is greatly increased.[17] For this reason, various complexes containing Gd^{3+} are widely used as T_1 contrast agents in practical applications.[18−21] On the other hand, the AIE phenomenon has gained increasing attention in the field of bioimaging.[22,23] Different from the fluorescence quenching of most planar fluorophores, the propeller-like AIE molecules do not emit or emit weakly in the molecular state due to the intramolecular rotation which consumes the absorbed energy.[13,14,24−26] However, strong emission may occur upon aggregation since the intramolecular rotations are restricted. Our study shows that, upon assembling the coordination complex of the Gd^{3+}-AIE ligand with a block copolymer, nanoparticles with MRI and FL dual performance may be produced.

In contrast to the employment of self-assembly in obtaining the dual-imaging nanoparticles, a lot of effort was made to fabricate various nanoparticles for single-mode MRI. Excellent examples include the dendronized iron oxide nanoparticles reported by Basly et al., the functionalized carbon nanotubes reported by Lamanna and Delogu et al., and so on. Obviously, these approaches require complicated preparation procedures, which is unfavorable for their applications. Moreover, the recent tendency in fabrication of dual MRI/FI dual imaging nanoparticles was to incorporate fluorescent quantum dots (QDs)[27] or organic dyes into iron oxide nanoparticles[2] or gadolinium chelates,[1,2,28] which further increases the difficulty in fabrication. On the contrary, the strategy of self-assembly reported in this work may greatly simplify the preparation procedure. We have reported in our previous work the formation of MRI/FI dual imaging micelles where the MRI and FI functions are originated from the coexistence of Gd^{3+} and Eu^{3+}.[18] In that case, the fluorescence is from the europium

Received: September 19, 2014
Revised: May 31, 2015
Published: July 6, 2015

DOI: 10.1021/acs.langmuir.5b01516
Langmuir 2015, 31, 7926−7933

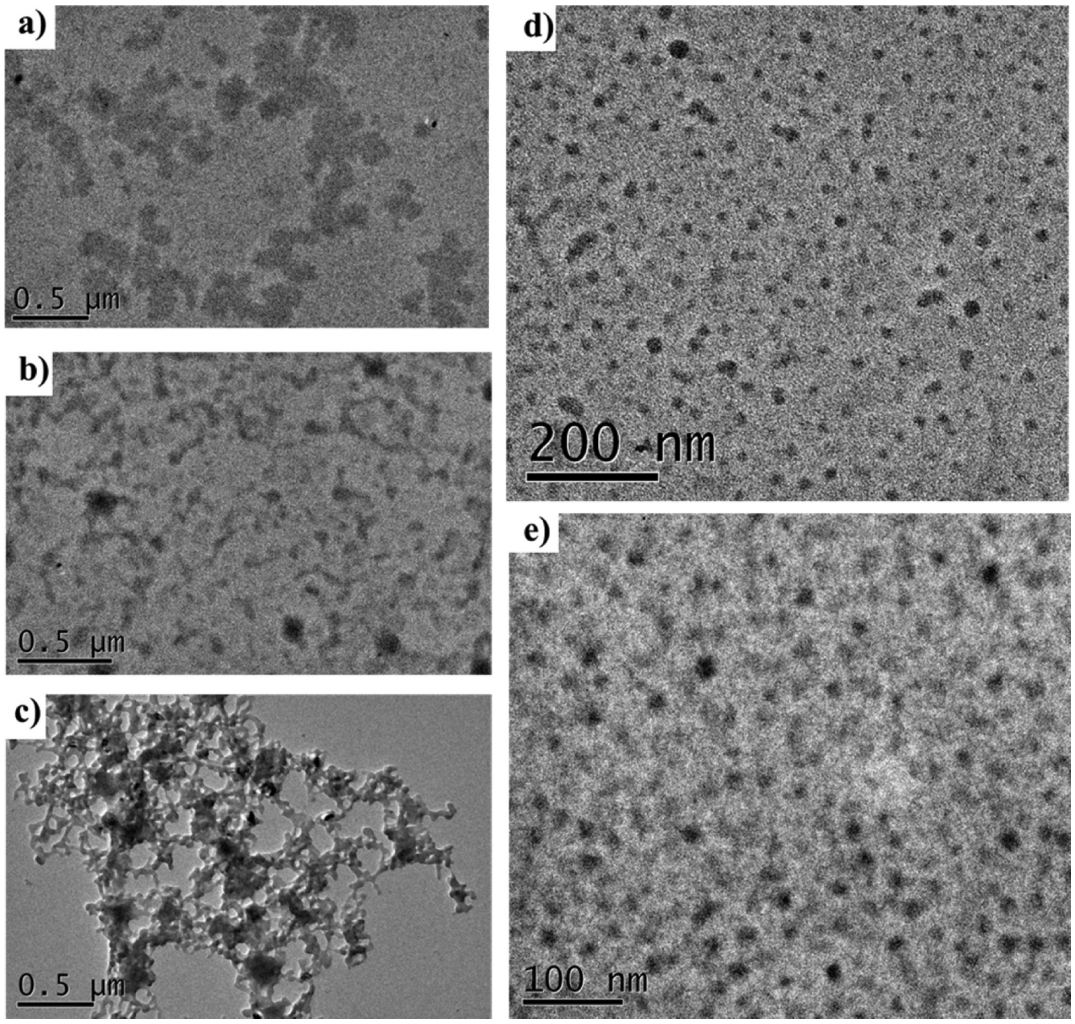

Figure 1. TEM images of the aggregates formed in the (a) TPE-(EO)4-L2 system, (b) TPE-(EO)4-L2/$PMVP_{41}$-PEO_{205} [+]/[−] = 1/2 system; (c) Gd^{3+}/TPE-(EO)4-L2 system; (d, e) [TPE-(EO)4-L2/Gd^{3+}/$PMVP_{41}$-PEO_{205}]−micelles system at different magnifications. In all these systems, [TPE-(EO)4-L2] = 0.3 mM.

ion, which requires excitation with UV light of 280 nm.[18] In the present work, the fluorescence is from the organic tetraphenyl ethylene (TPE) group, which allows excitation with visible light in practical biological operation.[29] Moreover, the dimension of the micelles is only about 40 nm, which is expected to facilitate their *in vitro* or *in vivo* applications.[27,30−33]

EXPERIMENTAL SECTION

1. Materials. *Synthesis of the Bifunctional Ligand TPE-(EO)4-L2.* TPE-(EO)4-L2 (L: dicarboxypyridine group) used in this work was synthesized according to previously reported procedures.[34]

Other Materials. Diblock polyelectrolyte poly(*N*-methyl-2-vinylpyridinium iodide)-*b*-poly(ethylene oxide) ($PMVP_{41}$-*b*-PEO_{205}, M_w = 19K, PDI = 1.05, about 90% quaternized) used in this work was prepared following a procedure described elsewhere.[35] Gadolinium nitrate, $Gd(NO_3)_3{\cdot}6H_2O$, was purchased from Aldrich and used without further purification. The other chemicals were obtained from Beijing Chemical Reagents Co. and all of A.R. grade. Distilled water was purified through a Milli-Q Advantage A10 ultrapure water system.

Sample Preparation. The desired amounts of TPE-(EO)4-L2 and $Gd(NO_3)_3$ were mixed in water in a glass vial. The final concentration of TPE-(EO)4-L2 and Gd^{3+} were 0.3 and 0.2 mM, respectively, to keep the ligand and metal ion at stoichiometric mixing ratio of ([TPE-(EO)4-L2]/[Gd^{3+}] = 3/2). In this way, each Gd^{3+} ion is expected to coordinate with three L groups, where L represents one head of the TPE-(EO)4-L2. The net charge calculated for each coordination center is −3, which means the concentration of negative charge [−] = 0.6 mM in the final mixtures. Then an equal volume of aqueous solution of $PMVP_{41}$-*b*-PEO_{205} with positive charges [+] = 0.6 mM was added, which made the [+] = [−] = 0.3 mM in the mixed systems. The pH for the final micellar system was adjusted to ∼7.4 using HCl and NaOH. All experiments were performed at room temperature (∼25 °C) unless otherwise specified.

2. Methods. *Transmission Electron Microscopy (TEM).* A FEI Tecnai G2 T20 TEM was employed to observe the morphology of micelles. Drops of samples were put onto 230 mesh copper grids coated with Formvar film. Excess water was removed by filter paper, and samples were then allowed to dry in ambient air at room temperature before TEM observation. The radius of the particles can be obtained directly on the basis of the given scaling bar. The average radius was obtained by averaging over 20 particles in the same figure.

Fluorescence Spectrometer Measurements. Steady-state fluorescence spectra were obtained with a Hitachi F-7000 fluorescence spectrometer. The emission wavelength was set at 480 nm, and the excitation wavelength was set at 366 nm. Emission spectra were recorded in the range of 375−700 nm. Excitation spectra were recorded in the range of 200−500 nm. The slit was set at 2.5 mm. The PMT voltage was 700 V, and the scan speed was 240 nm/min.

Dynamic Light Scattering Measurements. DLS measurements were carried out using a spectrometer of standard design (ALV-5000/E/WIN multiple tau digital correlator) with a Spectra-Physics 2017 22

DOI: 10.1021/acs.langmuir.5b01516
Langmuir 2015, 31, 7926−7933

Scheme 1. (a) Structure of TPE-(EO)4-L2; (b) Structure of $PMVP_{41}$-PEO_{205}; (c) Formation of [TPE-(EO)4-L2/Gd^{3+}/$PMVP_{41}$-PEO_{205}]−Micelles (Red Dots Represent Gd^{3+} Ions)

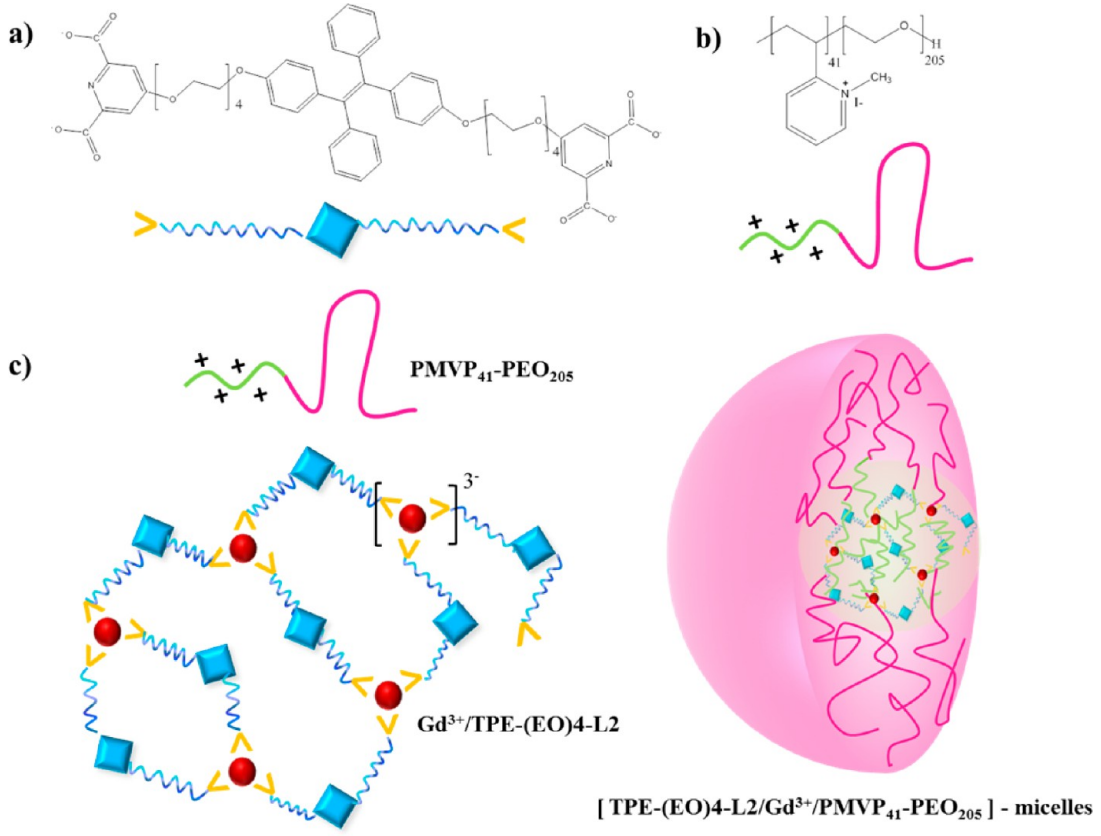

mW Ar laser (wavelength: 632.8 nm). The temperature was controlled at 25 ± 0.5 °C using a Haake C35 thermostat. To prepare dust-free solutions for light scattering measurements, the solutions were filtered through a 0.45 μm membrane of hydrophilic PVDF filter into light scattering cells before the measurements. The scattering angle was 90°, and the intensity autocorrelation functions were analyzed by using the method of CONTIN.[36,37]

Water Proton Relaxation Measurements. The longitudinal relaxation rates $1/T_1$ (R_1) were measured on the Bruker Avance 600 MHz spectrometer at 25 °C. The data points were collected with 16 transients and a recycle delay of 25 s. The delays used for R_1 experiments were 1, 50,100, 200, 300, 500, 800, 1000, 1500, 2000, 2500, 3000, 3500, 4000, 4500, and 5000 ms. The relaxation rate constants were obtained by fitting the peak intensities to a single-exponential function using the nonlinear least-squares method.

Confocal Fluorescent Images of Living Cell. All cells were incubated in complete medium (Dulbecco's modified Eagle's Medium, supplemented with 10% fetal bovine serum (FBS) and 1% penicillin−streptomycin) at 37 °C in an atmosphere containing 5% CO_2. For imaging, HeLa cells were grown in poly-D-lysine-coated dishes and incubated in 2 mL of complete medium for 24 h. Cells were washed with PBS, and the stocked [TPE-(EO)4-L2/Gd^{3+}/$PMVP_{41}$-PEO_{205}] mixed system was added to obtain a final concentration of 5 μM. The treated cells were incubated for another 12 h in the dark at 37 °C. A few minutes prior to confocal imaging cells were washed twice with PBS. A confocal laser scanning microscope (A1R-si, Nikon, Japan) was used to obtain images. Cells were imaged via the fluorescence mode with a 60× immersion lens with the following parameters: laser power 100%, pinhole 2.0 AU, excitation wavelength 405 nm, detector slit 425−475 nm and 552−617 nm, resolution 1024 × 1024, and a scan speed 0.5 frame/s.

Cytotoxicity Assay. Cell viability was determined by MTT assay.[38] Hela cells were seeded into a 96-well culture plate at a density of 5 × 10^3 cells $well^{-1}$ and cultured for 24 h in a 5% CO_2 incubator at 37 °C. Stock solutions of [TPE-(EO)4-L2/Gd^{3+}/$PMVP_{41}$-PEO_{205}]-micelles was prepared. The cells were treated with[TPE-(EO)4-L2/Gd^{3+}/$PMVP_{41}$-PEO_{205}] micelles at 0−50 μM or vehicle control for 12 h; the cell viability was measured by a microplate reader at 490 nm with the MTT staining assay. Optical density (OD) was read at 490 nm and subtracted background at 630 nm using a spectrophotometer (Multiskan MK3, Thermo Scientific, USA). Cell viability was expressed as a percentage of the corresponding control value. The data are expressed as the average of five replicates ± standard deviations (SD).

Magnetic Resonance Imaging (MRI). A 7T MRI system (Agilent, USA) was used for imaging. A spin-echo sequence was used with TR 500 ms and TE 14.7 ms to get T1 image.

RESULTS AND DISCUSSION

1. Formation of Hierarchical Micelles in the [TPE-(EO)4-L2/Gd^{3+}/$PMVP_{41}$-PEO_{205}] Mixed Systems. First we studied the solution behavior of TPE-(EO)4-L2. Although this bisligand molecule contains eight EO groups, it can be solublized in water only at pH >10.0. The "solution" of TPE-(EO)4-L2 exhibits Tyndall phenomenon, suggesting the presence of colloidal particles. TEM observations indicate the particles are ill-defined (Figure 1a). Meanwhile, fluorescence detection suggests the system is weakly emissive. These information indicates that the TPE-(EO)4-L2 molecules are not closely aggregated in the particles. We expect that the aggregates are probably loose clusters of TPE-(EO)4-L2 since the K^+ ions in the system may act as cross-linkers between the EO groups. However, upon addition of Gd^{3+}, precipitates form gradually which gives intensive emission. Obviously, the coordination between Gd^{3+} and TPE-(EO)4-L2 had triggered the aggregation of TPE-(EO)4-L2 which led to AIE. TEM

DOI: 10.1021/acs.langmuir.5b01516
Langmuir 2015, 31, 7926−7933

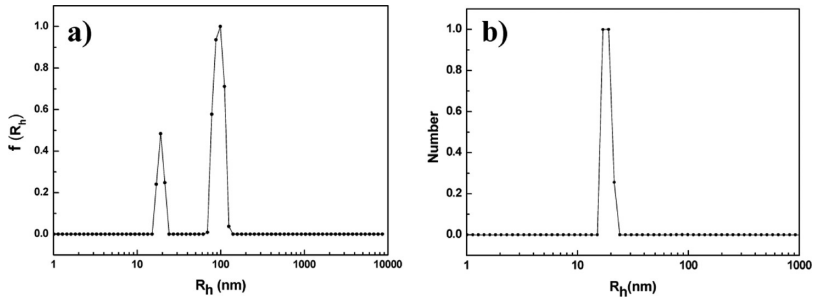

Figure 2. (a) Scattering intensity and (b) the number of particles as a function of hydrodynamic radius (R_h) distributions.

image reveals that the precipitates are network structures, suggesting the formation of coordination polymers between TPE-(EO)4-L2 and Gd^{3+} (Figure 1c). However, this network precipitates can be avoided if the same amount Gd^{3+} solution is added into the TPE-(EO)4-L2/$PMVP_{41}$-PEO_{205} mixed solution. Without Gd^{3+}, ill-defined structures are formed in this mixed system (Figure 1b), but well-defined micelles are formed immediately upon addition of Gd^{3+} (Figure 1d,e). This is in clear contrast with the precipitates in the coordinating system of TPE-(EO)4-L2/Gd^{3+}. It should be noted that the precipitates cannot be changed into micelles if $PMVP_{41}$-PEO_{205} is added to the TPE-(EO)4-L2/Gd^{3+} mixed system. Obviously, this three-component system has strong history effect that depends on the mixing order, as is completely different from the micelles based on coordination polymers in our previous study.[39−43] The formation of the hierarchical micelles is illustrated in Scheme 1.

The hydrodynamic radius of the micelles is further analyzed with DLS. Two groups of particles with average radius around 20 and 100 nm are observed. (Figure 2a). Since the scattering intensity is proportional to R^4, where R is the particle radius, the number of larger particles is actually negligible. This is confirmed by the number-averaged analysis (Figure 2b), where the peak for the particles around 100 nm vanishes completely; the particles with average radius around 20 nm are predominant in this system. The narrow peak width at 20 nm suggests that the micellar size is very homogeneous, which is in good agreement with the TEM observations. According to the TEM, the radius of the micellar core is about 7 nm, suggesting the thickness of the PEO corona surrounding the core is about 13 nm. This is also in good agreement with our previous results.[41,42] It can be inferred that the larger particles are produced by the deviation from the charge balance or coordination stoichiometry due to experimental errors.

2. Fluorescence Performance of the [TPE-(EO)4-L2/Gd^{3+}/$PMVP_{41}$-PEO_{205})] System. First, we checked the effect of Gd^{3+} and $PMVP_{41}$-PEO_{205} on the excitation spectrum of TPE-(EO)4-L2. The excitation maximum for both systems appears at 366 nm, suggesting both the Gd^{3+} and $PMVP_{41}$-PEO_{205} have not interacted with the ground state of the TPE group (Figure 3a).

The emission spectra of TPE-(EO)4-L2 at various conditions are shown in Figure 3b. In all cases, the spectra display a broad peak centered at around 475 nm (Figure 3b), but the emission intensity varies in the presence of Gd^{3+} and $PMVP_{41}$-PEO_{205}. It is noted that the emission of TPE-(EO)4-L2 is enhanced significantly upon addition of Gd^{3+}, but the emission in the TPE-(EO)4-L2/Gd^{3+} system is decreased about 10% after addition of $PMVP_{41}$-PEO_{205} block copolymer to balance the charges in the coordinating system. We infer that this is

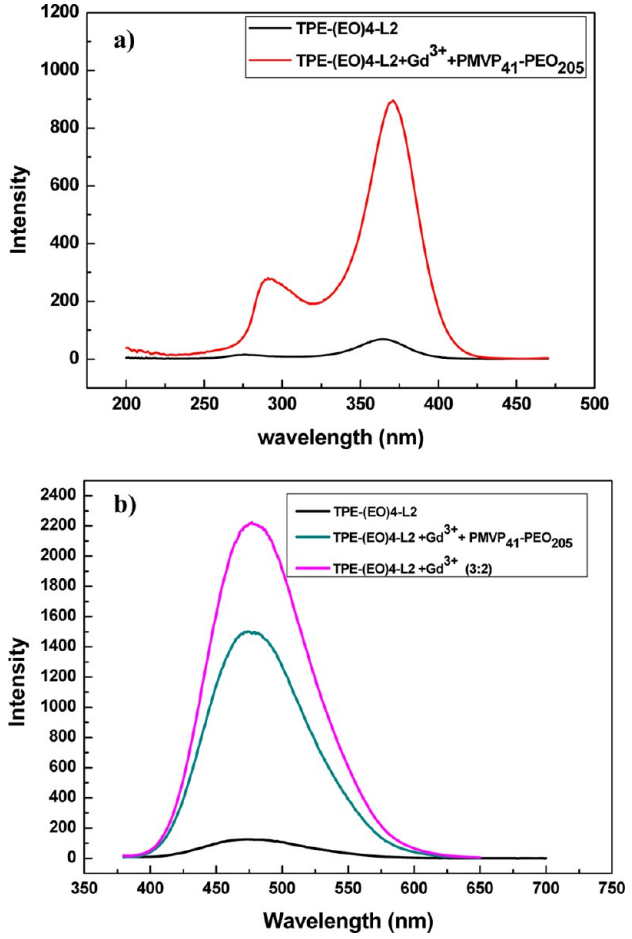

Figure 3. (a) Excitation fluorescence spectra of TPE-(EO)4-L2 (emission wavelength = 480 nm, [TPE-(EO)4-L2] = 0.3 mM) and the excitation fluorescence spectra of TPE-(EO)4-L2/Gd^{3+}/$PMVP_{41}$-PEO_{205} (emission wavelength = 480 nm, [TPE-(EO)4-L2] = 0.3 mM). (b) Emission fluorescence spectra of systems with different components, in which the [TPE-(EO)4-L2] was all fixed at 0.3 mM. Excitation wavelength = 366 nm.

probably caused by the different structures of the coordination complex in these two states. It is known that the AIE property is originated from the RIR (restriction of intramolecular rotations). Without the presence of $PMVP_{41}$-PEO_{205}, TPE-(EO)4-L2/Gd^{3+} complexes exist in the form of giant network structures up to several micrometers, yet the size of the network has been reduced to within 10 nm in the core of the micelles in the presence of $PMVP_{41}$-PEO_{205}. Obviously, the rotation of TPE-(EO)4-L2 molecules in the giant network structure is more difficult than that in the micelles, since the

DOI: 10.1021/acs.langmuir.5b01516
Langmuir 2015, 31, 7926−7933

latter allows more lateral TPE-(EO)4-L2 which has more rotation freedom. It is also possible that the formation of micelles may scatter some light which is to excite the TPE groups. Nevertheless, the emission in the micelles is strong enough to obtain a visible signal at micromolar level.

3. Cellular Fluorescence Imaging. In this section, we explored the fluorescence imaging property of the [TPE-(EO)4-L2/Gd^{3+}/$PMVP_{41}$-PEO_{205}]−micelles system. These micelles can be taken up by HeLa cells. Figure 4b shows that

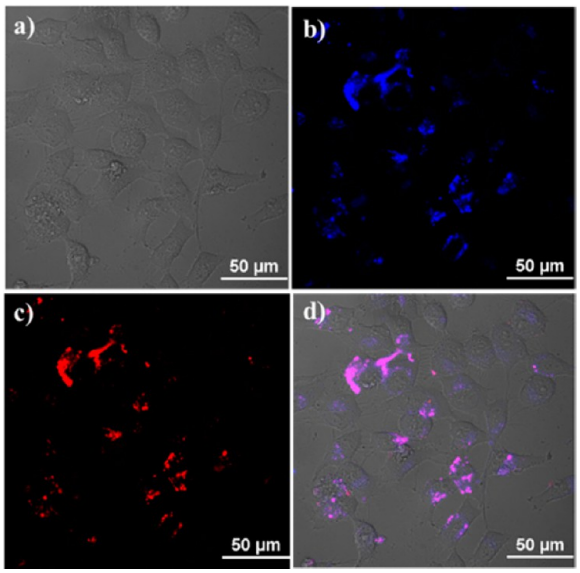

Figure 4. Confocal fluorescence images of living HeLa cells incubated with [TPE-(EO)4-L2/Gd^{3+}/$PMVP_{41}$-PEO_{205}]−micelles systems: (a) bright-field image, (b) detector slit 425−475 nm, (c) detector slit 552−617 nm, (d) overlap of (b) and (c). [TPE-(EO)4-L2] = 5 μM.

upon excitation with the 405 nm laser blue emission (425−475 nm) can be observed after the HeLa cells were incubated in the micellar system. Most interestingly, we found dual-channel fluorescence in the incubated HeLa cells under the same excitation. It is show in Figure 4c that red fluorescence (552−617 nm) can be obtained as well. Recently, dual fluorescence has attracted intensive attention toward improved fluorescence imaging.[43,44] Usually, dual-channel fluorescence can only be obtained by incorporating different fluorophores into the fluorescence probes.[43−45] Yet the mechanism of this two-channel fluorescence is probably caused by scattering of the micelles, since the appeared reports for TPE fluorophores never show such a phenomenon.[29,46−49] Anyway, this two-channel fluorescence in our [TPE-(EO)4-L2/Gd^{3+}/$PMVP_{41}$-PEO_{205}]−micellar systems is very interesting since it allows a more accurate imaging.

It should be mentioned that the [TPE-(EO)4-L2/Gd^{3+}/$PMVP_{41}$-PEO_{205}]−micelles systems could still form stable micelles in PBS solution which is the cell culture at low concentration (even 5 μM) (Figure 5a). Since cytotoxicity of [TPE-(EO)4-L2/Gd^{3+}/$PMVP_{41}$-PEO_{205}]−micelles systems is negligible to cells (Figure 5b), they are expected to be potentially used in *in vitro* applications.

4. Magnetic Resonance Imaging (MRI). Next we examine the magnetic resonance imaging (MRI) ability of the micelles. In general, with the same imaging parameters, the higher the concentration of the contrast agent is the larger the change of water relaxation in tissue is. At low concentrations,

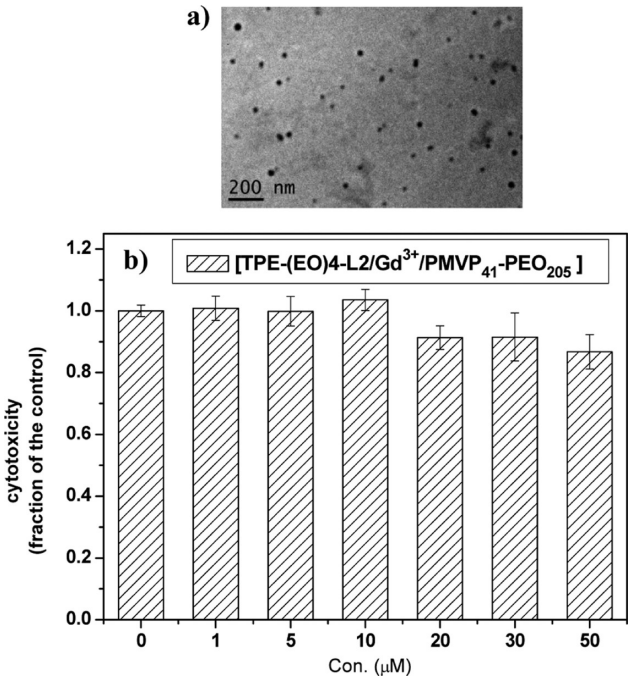

Figure 5. (a) TEM image of [TPE-(EO)4-L2/Gd^{3+}/$PMVP_{41}$-PEO_{205}]−micelles in PBS solution which is the cell culture at 5 μM. (b) Cytotoxicity of [TPE-(EO)4-L2/Gd^{3+}/$PMVP_{41}$-PEO_{205}]−micelles to HeLa cells.

contrast agent-induced tissue relaxivity obeys the linear relationship (take T_1-weighted MRI for example),[17] i.e.

$$R_1 = R_1^0 + r_1 CA \quad (1)$$

where R_1^0 is the tissue relaxivity in the absence of contrast agent (CA). R_1^0 varies with tissue type and the applied field. The ionic relaxivity rate, r_1 (with units in mM^{-1} s^{-1}), of a contrast agent describes its capacity for contrast enhancement. It is known that Gd^{3+} is the strongest paramagnetic species owing to the presence of seven unpaired electrons. It is found that the spin−lattice relaxation time T_1 of water was considerably decreased in the TPE-(EO)4-L2/Gd^{3+}/$PMVP_{41}$-PEO_{205} micellar system. Figure 6 demonstrates that $1/T_1$ increases linearly with increasing the concentration of the Gd^{3+}-micelles (expressed in the concentration of Gd^{3+} ions).

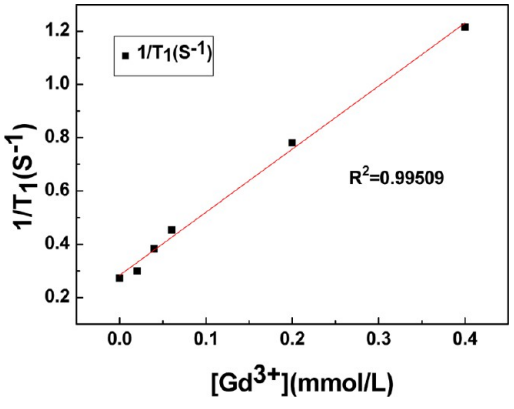

Figure 6. NMR relaxation times of the protons in water influenced by the [TPE-(EO)4-L2/Gd^{3+}/$PMVP_{41}$-PEO_{205})]−micelles.

DOI: 10.1021/acs.langmuir.5b01516
Langmuir 2015, 31, 7926−7933

From Figure 6 we can find that the [TPE-(EO)4-L2/Gd^{3+}/$PMVP_{41}$-PEO_{205})]−micelles are T_1-weighted contrast agents. According to eq 1

$$R_1 = 0.284 + 2.37[Gd^{3+}]r_1 = 2.37\ (mM_{Gd}\ s)^{-1}$$

The relaxivity was found to be 2.37 mM^{-1} Gd^{-1} s^{-1}(600 MHz, 25 °C). Since one micelle always contains hundreds of ions, the relaxivity of one micelle could be ∼10^3 mM^{-1} $micelle^{-1}$ s^{-1} (600 MHz, 25 °C), which is comparable with literature reports.[17,50]

The effective change of the T_1 value of water using the [TPE-(EO)4-L2/Gd^{3+}/$PMVP_{41}$-PEO_{205}]−micelles allows us to perform *in vitro* MRI experiments. Figure 7a,b compares the T_1 contrast MRI image of water without and with the presence of TPE-(EO)4-L2/Gd^{3+}/$PMVP_{41}$-PEO_{205}-micelles. It can be clearly observed in Figure 7 that the MRI contrast in map b, which corresponds to the micellar system, is fairly good, whereas that for map a, which is made with pure water, is rather poor. Obviously, the contrast with the presence of [TPE-(EO)4-L2/Gd^{3+}/$PMVP_{41}$-PEO_{205}]−micelles (Figure 7b) is significantly enhanced, confirming the effective MRI ability.

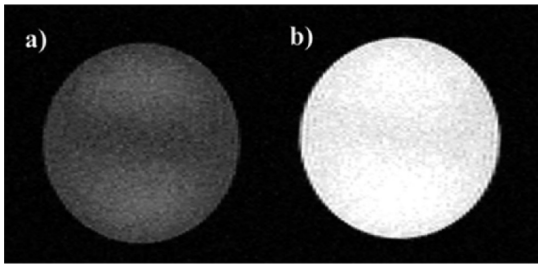

Figure 7. MRI results of (a) water and (b) TPE-(EO)4-L2/Gd^{3+}/$PMVP_{41}$-PEO_{205}−micelles system; [TPE-(EO)4-L2] = 0.3 mM).

5. Salt Effect. The MRI-FL dual imaging [TPE-(EO)4-L2/Gd^{3+}/$PMVP_{41}$-PEO_{205}]−micelles hold great promise from the application point of view, so we further investigated the stability of the micellar structures at high salt concentrations. Polyion micelles typically strongly respond to ionic strength; hence, we studied the effect of salt on the micelles. Figure 8 shows the light scattering intensity and hydrodynamic radius of micelles as a function of salt concentration. Remarkably, the intensity and the radius nearly do not change up to 200 mM NaCl for a micellar solution with [TPE-(EO)4-L2] as low as 5 μM. It is thus likely that the high stability of [TPE-(EO)4-L2/Gd^{3+}/$PMVP_{41}$-PEO_{205}]−micelles is due to the branched structure and the high negative charge of Gd^{3+}/TPE complexes formed at a 2/3 ratio with three tridentate ligand moieties coordinating to a single Gd^{3+}ion. Since the biological salt concentration is about 150 mM, the excellent stability of the micelles at 200 mM NaCl suggests the robust potential of the [TPE-(EO)4-L2/Gd^{3+}/$PMVP_{41}$-PEO_{205}]−micelles in future applications such as advanced MRI/FL dual imaging.

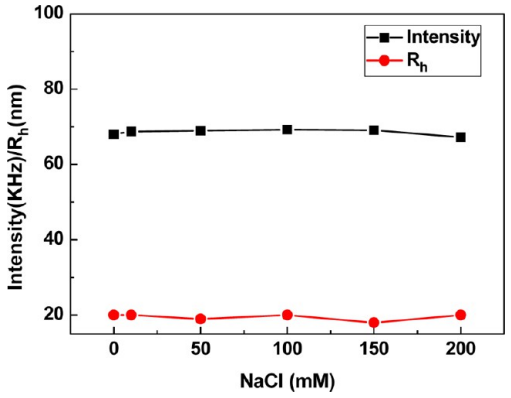

Figure 8. Effect of salt concentration on scattering intensity and size of [TPE-(EO)4-L2/Gd^{3+}/$PMVP_{41}$-PEO_{205}]−micelles. The concentration of the [TPE-(EO)4-L2] = 5 μM.

CONCLUSION

In conclusion, we reported a new micellar system that exhibits fluorescence and MRI bimodal functions via combining the Gd^{3+} and aggregation induced emission (AIE) group into the micelles. The micelles display excellent stability in biological salt environment and show negligible cytotoxity toward HeLa cells. Upon endocytosis into the HeLa cells, the micelles display dual channel fluorescence in the range of 425−475 and 552−617 nm, respectively. Meanwhile, the presence of micelles can considerably increase the T_1 signal of water. Taking into account the easy preparation nature of the electrostatic self-assembly, we expect this micellar system may have great potential in biomedical applications, given that *in vivo* imaging experiments were successful as the *in vitro* ones in this work.

AUTHOR INFORMATION

Corresponding Authors

*E-mail yunyan@pku.edu.cn (Y.Y.).
*E-mail jbhuang@pku.edu.cn (J.H.).

Notes

The authors declare no competing financial interest.

ACKNOWLEDGMENTS

This work is supported by National Natural Science Foundation of China (21422302, 21173011, 21273013, 51121091), National Basic Research Program of China (973 Program, 2013CB933800), and Doctoral Program of Higher Education of China. We thank Dr. Xinyuan Xu, Professor Huwei Liu, and Yu Bai for the cytotoxity experiments.

REFERENCES

(1) Zheng, J.-P.; Zhen, M.-M.; Wang, C.-R.; Shu, C.-Y. Recent Progress of Molecular Imaging Probes Based on Gadofullerenes. *Chin. J. Anal. Chem.* **2012**, *40*, 1607−1614.

(2) Lim, Y. T.; Noh, Y.-W.; Han, J. H.; Cai, Q.-Y.; Yoon, K.-H.; Chung, B. H. Biocompatible Polymer-Nanoparticle-Based Bimodal Imaging Contrast Agents for the Labeling and Tracking of Dendritic Cells. *Small* **2008**, *4*, 1640−1645.

(3) Basly, B.; Felder-Flesch, D.; Perriat, P.; Billotey, C.; Taleb, J.; Pourroy, G.; Begin-Colin, S. Dendronized Iron Oxide Nanoparticles as Contrast Agents for MRI. *Chem. Commun.* **2010**, *46*, 985−987.

(4) Lamanna, G.; Garofalo, A.; Popa, G.; Wilhelm, C.; Begin-Colin, S.; Felder-Flesch, D.; Bianco, A.; Gazeau, F.; Menard-Moyon, C. Endowing Carbon Nanotubes with Superparamagnetic Properties: Applications for Cell Labeling, MRI Cell Tracking and Magnetic Manipulations. *Nanoscale* **2013**, *5*, 4412−4421.

(5) Yun, S.-W.; Leong, C.; Bi, X.; Ha, H.-H.; Yu, Y. H.; Tan, Y. L.; Narayanan, G.; Sankaran, S.; Kim, J.-Y.; Hariharan, S.; Ahmed, S.; Chang, Y.-T. A Fluorescent Probe for Imaging Symmetric and Asymmetric Cell Division in Neurosphere Formation. *Chem. Commun.* **2014**, *50*, 7492−7494.

(6) Erlichman, D. B.; Blitman, N.; Weinstein, S.; Taragin, B. Use of Multidetector Computed Tomography 3D Reconstructions in

DOI: 10.1021/acs.langmuir.5b01516
Langmuir 2015, 31, 7926−7933

Assessing Lower Tracheal-bronchial Pathology and Subsequent Surgical Interventions. *Clin. imaging.* **2015**, *39*, 259−63.
(7) Delogu, L. G.; Vidili, G.; Venturelli, E.; Menard-Moyon, C.; Zoroddu, M. A.; Pilo, G.; Nicolussi, P.; Ligios, C.; Bedognetti, D.; Sgarrella, F.; Manetti, R.; Bianco, A. Functionalized Multiwalled Carbon Nanotubes as Ultrasound Contrast Agents. *Proc. Natl. Acad. Sci. U. S. A.* **2012**, *109*, 16612−16617.
(8) Yue, B.; Tang, T. The Use of Nuclear Imaging for the Diagnosis of Periprosthetic Infection after Knee and Hip Arthroplasties. *Nucl. Med. Commun.* **2015**, *36*, 305−11.
(9) Frullano, L.; Meade, T. J. Multimodal MRI Contrast Agents. *JBIC, J. Biol. Inorg. Chem.* **2007**, *12*, 939−949.
(10) Bonnet, C. S.; Toth, E. Towards Highly Efficient, Intelligent and Bimodal Imaging Probes: Novel Approaches Provided by Lanthanide Coordination Chemistry. *C. R. Chim.* **2010**, *13*, 700−714.
(11) Pellegatti, L.; Zhang, J.; Drahos, B.; Villette, S.; Suzenet, F.; Guillaumet, G.; Petoud, S.; Toth, E. Pyridine-based Lanthanide Complexes: Towards Bimodal Agents Operating as Near Infrared Luminescent and MRI Reporters. *Chem. Commun.* **2008**, 6591−6593.
(12) Mulder, W. J. M.; Griffioen, A. W.; Strijkers, G. J.; Cormode, D. P.; Nicolay, K.; Fayad, Z. A. Magnetic and Fluorescent Nanoparticles for Multimodality Imaging. *Nanomedicine* **2007**, *2*, 307−324.
(13) Hong, Y.; Lam, J. W. Y.; Tang, B. Z. Aggregation-induced Emission: Phenomenon, Mechanism and Applications. *Chem. Commun.* **2009**, 4332−4353.
(14) Hong, Y.; Lam, J. W. Y.; Tang, B. Z. Aggregation-induced Emission. *Chem. Soc. Rev.* **2011**, *40*, 5361−5388.
(15) Liu, J.; Zhong, Y.; Lu, P.; Hong, Y.; Lam, J. W. Y.; Faisal, M.; Yu, Y.; Wong, K. S.; Tang, B. Z. A Superamplification Effect in the Detection of Explosives by a Fluorescent Hyperbranched poly-(silylenephenylene) with Aggregation-enhanced Emission Characteristics. *Polym. Chem.* **2010**, *1*, 426−429.
(16) Villaraza, A. J. L.; Bumb, A.; Brechbiel, M. W. Macromolecules, Dendrimers, and Nanomaterials in Magnetic Resonance Imaging: The Interplay between Size, Function, and Pharmacokinetics. *Chem. Rev.* **2010**, *110*, 2921−2959.
(17) Bruckman, M. A.; Yu, X.; Steinmetz, N. F. Engineering Gd-loaded Nanoparticles to Enhance MRI Sensitivity viaT1Shortening. *Nanotechnology* **2013**, *24*, 462001.
(18) Wang, J. Y.; Velders, A. H.; Gianolio, E.; Aime, S.; Vergeldt, F. J.; Van As, H.; Yan, Y.; Drechsler, M.; de Keizer, A.; Cohen Stuart, M. A.; van der Gucht, J. Controlled Mixing of Lanthanide(III) Ions in Coacervate Core Micelles. *Chem. Commun.* **2013**, *49*, 3736−3738.
(19) Torres, S.; Martins, J. A.; Andre, J. P.; Geraldes, C.; Merbach, A. E.; Toth, E. Supramolecular Assembly of an Amphiphilic Gd-III Chelate: Tuning the Reorientational Correlation Time and the Water Exchange Rate. *Chem. - Eur. J.* **2006**, *12*, 940−948.
(20) Sitharaman, B.; Kissell, K. R.; Hartman, K. B.; Tran, L. A.; Baikalov, A.; Rusakova, I.; Sun, Y.; Khant, H. A.; Ludtke, S. J.; Chiu, W.; Laus, S.; Toth, E.; Helm, L.; Merbach, A. E.; Wilson, L. J. Superparamagnetic Gadonanotubes are High-performance MRI Contrast Agents. *Chem. Commun.* **2005**, 3915−3917.
(21) Colombo, M.; Carregal-Romero, S.; Casula, M. F.; Gutierrez, L.; Morales, M. P.; Boehm, I. B.; Heverhagen, J. T.; Prosperi, D.; Parak, W. J. Biological Applications of Magnetic Nanoparticles. *Chem. Soc. Rev.* **2012**, *41*, 4306−4334.
(22) Wang, M.; Zhang, G.; Zhang, D.; Zhu, D.; Tang, B. Z. Fluorescent Bio/chemosensors Based on Silole and Tetraphenylethene Luminogens with Aggregation-induced Emission Feature. *J. Mater. Chem.* **2010**, *20*, 1858−1867.
(23) Wu, W.-C.; Chen, C.-Y.; Tian, Y.; Jang, S.-H.; Hong, Y.; Liu, Y.; Hu, R.; Tang, B. Z.; Lee, Y.-T.; Chen, C.-T.; Chen, W.-C.; Jen, A. K. Y. Enhancement of Aggregation-Induced Emission in Dye-Encapsulating Polymeric Micelles for Bioimaging. *Adv. Funct. Mater.* **2010**, *20*, 1413−1423.
(24) Zhao, Z.; Chen, S.; Shen, X.; Mahtab, F.; Yu, Y.; Lu, P.; Lam, J. W. Y.; Kwok, H. S.; Tang, B. Z. Aggregation-induced Emission, Self-assembly, and Electroluminescence of 4,4′-bis(1,2,2-triphenylvinyl)-biphenyl. *Chem. Commun.* **2010**, *46*, 686−688.
(25) Zhao, Z.; Wang, Z.; Lu, P.; Chan, C. Y. K.; Liu, D.; Lam, J. W. Y.; Sung, H. H. Y.; Williams, I. D.; Ma, Y.; Tang, B. Z. Structural Modulation of Solid-State Emission of 2,5-Bis(trialkylsilylethynyl)-3,4-diphenylsiloles. *Angew. Chem., Int. Ed.* **2009**, *48*, 7608−7611.
(26) Zheng, Y.-S.; Hu, Y.-J. Chiral Recognition Based on Enantioselectively Aggregation-Induced Emission. *J. Org. Chem.* **2009**, *74*, 5660−5663.
(27) Maldiney, T.; Richard, C.; Seguin, J.; Wattier, N.; Bessodes, M.; Scherman, D. Effect of Core Diameter, Surface Coating, and PEG Chain Length on the Biodistribution of Persistent Luminescence Nanoparticles in Mice. *ACS Nano* **2011**, *5*, 854−862.
(28) Manus, L. M.; Mastarone, D. J.; Waters, E. A.; Zhang, X.-Q.; Schultz-Sikma, E. A.; MacRenaris, K. W.; Ho, D.; Meade, T. J. Gd(III)-Nanodiamond Conjugates for MRI Contrast Enhancement. *Nano Lett.* **2010**, *10*, 484−489.
(29) Qin, W.; Ding, D.; Liu, J. Z.; Yuan, W. Z.; Hu, Y.; Liu, B.; Tang, B. Z. Biocompatible Nanoparticles with Aggregation-Induced Emission Characteristics as Far-Red/Near-Infrared Fluorescent Bioprobes for In Vitro and In Vivo Imaging Applications. *Adv. Funct. Mater.* **2012**, *22*, 771−779.
(30) Yildirimer, L.; Thanh, N. T. K.; Loizidou, M.; Seifalian, A. M. Toxicological Considerations of Clinically Applicable Nanoparticles. *Nano Today* **2011**, *6*, 585−607.
(31) Shellock, F. G.; Kanal, E. Safety of Magnetic Resonance Imaging Contrast Agents. *J. Magn. Reson. Imaging* **1999**, *10*, 477−484.
(32) Peer, D. Immunotoxicity Derived from Manipulating Leukocytes with Lipid-based Nanoparticles. *Adv. Drug Delivery Rev.* **2012**, *64*, 1738−1748.
(33) Geng, Y.; Dalhaimer, P.; Cai, S.; Tsai, R.; Tewari, M.; Minko, T.; Discher, D. E. Shape Effects of Filaments Versus Spherical Particles in Flow and Drug Delivery. *Nat. Nanotechnol.* **2007**, *2*, 249−255.
(34) Xu, L.; Jiang, L.; Drechsler, M.; Sun, Y.; Liu, Z.; Huang, J.; Tang, B. Z.; Li, Z.; Cohen Stuart, M. A.; Yan, Y. Self-Assembly of Ultralong Polyion Nanoladders Facilitated by Ionic Recognition and Molecular Stiffness. *J. Am. Chem. Soc.* **2014**, *136*, 1942−1947.
(35) Harada, A.; Kataoka, K. Novel Polyion ComplexMicelles Entrapping Enzyme Molecules in the Core: Preparation of Narrowly-distributed Micelles from Lysozyme and poly(ethylene glycol)-poly(aspartic acid) Block Copolymer in Aqueous Medium. *Macromolecules* **1998**, *31*, 288−294.
(36) Provencher, S. W. A Constrained Regularization Method for Inverting Data Represented by= Linear Algebraic or Integral-equations. *Comput. Phys. Commun.* **1982**, *27*, 213−227.
(37) Provencher, S. W. Contin - a General-purpose Constrained Regularization Program for Inverting Noisy Linear Algebraic and Integral-equations. *Comput. Phys. Commun.* **1982**, *27*, 229−242.
(38) Ferrari, M.; Fornasiero, M. C.; Isetta, A. M. MTT Colorimrtric Assay for Testing Macrophage Cytotoxic Activity Invitro. *J. Immunol. Methods* **1990**, *131*, 165−172.
(39) Yan, Y.; Lan, Y. R.; de Keizer, A.; Drechsler, M.; Van As, H.; Cohen Stuart, M. A.; Besseling, N. A. M. Redox Responsive Molecular Assemblies Based on Metallic Coordination Polymers. *Soft Matter* **2010**, *6*, 3244−3248.
(40) Yan, Y.; Harnau, L.; Besseling, N. A. M.; de Keizer, A.; Ballauff, M.; Rosenfeldt, S.; Cohen Stuart, M. A. Spherocylindrical Coacervate Core Micelles Formed by a Supramolecular Coordination Polymer and a Diblock Copolymer. *Soft Matter* **2008**, *4*, 2207−2212.
(41) Yan, Y.; Besseling, N. A. M.; de Keizer, A.; Marcelis, A. T. M.; Drechsler, M.; Cohen Stuart, M. A. Hierarchical Self-assembly in Solutions Containing Metal Ions, Ligand, and Diblock Copolymer. *Angew. Chem., Int. Ed.* **2007**, *46*, 1807−1809.
(42) Zhao, L.; Yan, Y.; Huang, J. Redox-Gated Potential Micellar Carriers Based on Electrostatic Assembly of Soft Coordination Suprapolymers. *Langmuir* **2012**, *28*, 5548−5554.
(43) Xu, L.; Feng, L.; Han, Y.; Jing, Y.; Xian, Z.; Liu, Z.; Huang, J.; Yan, Y. Supramolecular Self-assembly Enhanced Europium(iii) luminescence under visible light. *Soft Matter* **2014**, *10*, 4686−4693.
(44) Lin, W.; Yuan, L.; Feng, J. A dual-channel Fluorescence-enhanced Sensor for Aluminum Ions Based on Photoinduced Electron

DOI: 10.1021/acs.langmuir.5b01516
Langmuir 2015, 31, 7926−7933

Transfer and Excimer Formation. *Eur. J. Org. Chem.* **2008**, *2008*, 3821−3825.
(45) Ma, T.-H.; Dong, M.; Dong, Y.-M.; Wang, Y.-W.; Peng, Y. A Unique Water-Tuning Dual-Channel Fluorescence-Enhanced Sensor for Aluminum Ions Based on a Hybrid Ligand from a 1,1 ’-Binaphthyl Scaffold and an Amino Acid. *Chem. - Eur. J.* **2010**, *16*, 10313−10318.
(46) Geng, J.; Liao, L. D.; Qin, W.; Tang, B. Z.; Thakor, N.; Liu, B. Fluorogens with Aggregation Induced Emission: Ideal Photoacoustic Contrast Reagents Due to Intramolecular Rotation. *J. Nanosci. Nanotechnol.* **2015**, *15*, 1864−1868.
(47) Song, Z. G.; Hong, Y. N.; Kwok, R. T. K.; Lam, J. W. Y.; Liu, B.; Tang, B. Z. A Dual-mode Fluorescence “turn-on” Biosensor Based on an Aggregation-induced Emission Luminogen. *J. Mater. Chem. B* **2014**, *2*, 1717−1723.
(48) Zhao, Q. L.; Li, K.; Chen, S. J.; Qin, A. J.; Ding, D.; Zhang, S.; Liu, Y.; Liu, B.; Sun, J. Z.; Tang, B. Aggregation-induced Red-NIR Emission Organic Nanoparticles as Effective and Photostable Fluorescent Probes for Bioimaging. *J. Mater. Chem.* **2012**, *22*, 15128−15135.
(49) Xu, L. M.; Jiang, L. X.; Drechsler, M.; Sun, Y.; Liu, Z. R.; Huang, J. B.; Tang, B. Z.; Li, Z. B.; Cohen Stuart, M. A.; Yan, Y. Self-Assembly of Ultralong Polyion Nanoladders Facilitated by Ionic Recognition and Molecular Stiffness. *J. Am. Chem. Soc.* **2014**, *136*, 1942−1947.
(50) Delli Castelli, D.; Gianolio, E.; Geninatti Crich, S.; Terreno, E.; Aime, S. Metal Containing Nanosized Systems for MR-Molecular Imaging Applications. *Coord. Chem. Rev.* **2008**, *252*, 2424−2443.

DOI: 10.1021/acs.langmuir.5b01516
Langmuir 2015, 31, 7926−7933